Acta Mech Sinica (2006) 22: 9–16
DOI 10.1007/s10409-005-0083-1

RESEARCH PAPER

Baolin Tian · Dexun Fu · Yanwen Ma

Numerical investigation of Richtmyer-Meshkov instability driven by cylindrical shocks*

Received: 12 January 2005 / Accepted: 4 August 2005 / Revised: 11 August 2005 / Published online: 10 January 2006

Abstract In this paper, a numerical method with high order accuracy and high resolution was developed to simulate the Richtmyer-Meshkov(RM) instability driven by cylindrical shock waves. Compressible Euler equations in cylindrical coordinate were adopted for the cylindrical geometry and a third order accurate group control scheme was adopted to discretize the equations. Moreover, an adaptive grid technique was developed to refine the grid near the moving interface to improve the resolution of numerical solutions. The results of simulation exhibited the evolution process of RM instability, and the effect of Atwood number was studied. The larger the absolute value of Atwood number, the larger the perturbation amplitude. The nonlinear effect manifests more evidently in cylindrical geometry. The shock reflected from the pole center accelerates the interface for the second time, considerably complicating the interface evolution process, and such phenomena of reshock and secondary shock were studied.

Keywords Richtmyer-Meshkov instability · Atwood number · cylindrical shock

1 Introduction

When two different fluids are impulsively accelerated together by a shock wave, small perturbations at the material interface grow linearly first, followed by the formation of nonlinear structures characterized by "spikes" and "bubbles", and then the mixing of fluids. Such a phenomenon is known as Richtmyer-Meshov(RM) instability. The instability was first predicted theoretically by Richtmyer in 1960 [1]. Ten years later, Meshkov confirmed Richtmyer's prediction experimentally [2].

RM instability plays an important role in the area of inertial confinement fusion (ICF). The mixing due to the instability at the interface is a restrictive factor for the energy gain generated in ICF. RM instability also takes place in many other natural and man-made phenomena, such as supernova, deflagration-to-detonation transition and so on. Moreover, the RM instability can induce turbulent mixing of fluids [3]. The research on the instability will be much helpful in understanding the mechanism of turbulence.

RM instability is closely related to Rayleigh-Taylor (RT) instability. They share certain common features, such as the formation and growth of bubbles and spikes. Here, the bubble is the portion of the light fluid penetrating into the heavy one. On the contrary, the spike is the portion of the heavy fluid penetrating into the light one. However, due to the different external forces, the two kinds of instabilities show different characteristics. The driving mechanism of RT is the presence of a uniform gravity field affecting both fluids, which gives rise to exponential growth in time in the regime of small amplitude. On the contrary, the RM problem is driven by shock wave and always unstable whether the shock wave comes from the heavy fluid towards the light fluid and collides with the interface or vice versa [4–6]. The initial deposition of vorticity at the interface controls the instability growth rate. This vorticity is modified later by the action of sound waves that are reflected at the shock and go back to catch up with the material interface.

The evolution of the instability has a closed relationship with the compressibility of the system. Therefore, RM instability is not exactly a kind of RT instability, and in fact the inherent compressibility physics is an important factor to take into account [7]. Combination of compressibility phenomena, such as shock interaction and refraction, with interface instability, including linear and nonlinear growth and subsequent transition to turbulence across a wide range of Mach numbers has been a challenge to theorists, experimentalists and computer modeler alike [7,8].

* The project supported by the National Natural Science Foundation of China (10176033, 10135010 and 90205025). The English text was polished by Yunming Chen.

B.L. Tian · D.X. Fu (✉) · Y.W. Ma
LNM, Institute of Mechanics, Chinese Academy of Sciences,
Beijing 100080, China
E-mail: fudx@lnm.imech.ac.cn

B.L. Tian
Institute of Applied Physics and Computational Mathematics,
Beijing 100088, China
E-mail: tian_baolin@iapcm.ac.cn

A number of linear and nonlinear theories have been developed based on various simplifications and approximations [1,2,4–6,9–17]. Impulsive models were widely used to describe the asymptotic growth rate in many experimental and theoretical works because of their simplicity [1,2, 10]. The explicit time dependence on the unperturbed state makes the linear stability analysis of RM instability considerably difficult. Fraley [5] and Yang et al.[4] advanced their linear theories based on the early work of Richtmyer [1]. Velikovich [18] developed an analytic theory of Richtmyer-Meshkov instability for the case of reflected rarefaction wave. However, most of the theories maintain valid only to some extent in the early and intermediate stages of RM instability. Then, some nonlinear theories have been developed to describe the evolution of the spikes and bubbles forming on the interface in later stage [15,16,19,20]. Meanwhile, many experiments have been designed to study the RM instability [7,8,13,20–23]. In recent years, with the aid of modern computers, numerical simulation has become a very helpful and powerful tool for the investigation of RM instability [3,7,13, 19,24–30].

Previous theoretical and numerical studies are mainly performed in planar geometry, i.e., the interaction between planar shock wave and perturbed planar interface, and many studies are restricted to two-dimensional cases. Recently, a few studies of 3D RM instabilities have been found. Cloutman and Wehner [25] simulated the RM instability of the interface between layers of air and either helium or SF_6 in both 2D and 3D cases by a finite difference method with a front-racking technique. Their results were found to agree well with experimental data except the initial instability growth rate. Li and Zhang [20] presented a numerical study of RM instability in two and three dimensions using a high resolution numerical method, and the solutions agree well with a recently developed nonlinear theory [17]. Oron et al.[31] investigated the difference between 2D and 3D case for the later stage evolution of RT and RM instability. Cohen et al.[3] performed 3D high-resolution simulation for a RM instability generated by a shock passing through a contact discontinuity with a two-scale initial perturbation, and their results suggests a mixing transition from unstable to turbulent flow as the numerical Reynolds number is increased. Compared with the results of single-scale perturbation, the coupling of the disparate scales leads to destruction of the small-scale bubbles and spikes. Zhou et al.[32] developed a robust, easy to apply criteria for the mixing transition in a time-dependent flow by the 3D DNS of RT and RM instability.

However, in most practical applications, such as ICF or supernova, RM instability occurs in a curved geometry, which complicates the system considerably. Firstly, the unperturbed system does not have analytical solution in a curved geometry, whereas the unperturbed system in the planar geometry does. Secondly, due to the curved geometry, the initial perturbation grows nonlinearly even in the early stage of RM instability. Moreover, the system is complicated by the re-acceleration of the material interface caused by the waves and shocks reflected back from the origin.

Now no analytic theory has been found for the RM instability in cylindrical or spherical case, and also there are only a few simulation results. Zhang and Graham [26] performed a numerical study of RM instability driven by cylindrical shocks for both the imploding and exploding cases for the air-SF_6 interface. Meanwhile, they [16] studied the scaling laws for unstable interfaces driven by strong shocks in a cylindrical geometry by numerical simulation incoporating the front tracking, and found a critical Mach number above which the scaling laws hold as a function of Atwood number, adiabatic exponents of the two fluids and geometry. By applying the front tracking, Dutta et al.[33,34] conducted numerical simulations of RM instabilities in spherical geometry for axisymmetric flow. They demonstrated scaling invariance with respect to the shock Mach number for fluid mixing statistics, such as growth rate and volume fraction.

In this paper, we present a detailed numerical investigation of RM instability in a cylindrical geometry driven by imploding shock waves. In Section 2, the numerical method (Eulerian cylindrical plus level set method plus discretization method) is discussed. In Section 3 a study on the Atwood number effect is presented, especially for the formation and growth of bubbles and spikes. Finally, a short summary is given in Section 4.

2 Numerical method

2.1 Governing equations

The following two-dimensional compressible dimensionless Euler equations in cylindrical coordinate are used to simulate RM instability with cylindrical shock-cylindrical interface interaction.

$$\frac{\partial \boldsymbol{W}}{\partial t}+\frac{\partial \boldsymbol{F}^{(e)}}{\partial r}+\frac{1}{r}\frac{\partial \boldsymbol{G}^{(e)}}{\partial \theta}=S_1, \tag{1}$$

where

$$W=[\rho,\rho u,\rho v,\rho E]^{\mathrm{T}},$$

$$F^{(e)}=\Big[\rho u,\rho u^2+p,\rho uv,\rho u\Big(E+\frac{p}{\rho}\Big)\Big]^{\mathrm{T}},$$

$$G^{(e)}=\Big[\rho v,\rho uv,\rho v^2+p,\rho u\Big(E+\frac{p}{\rho}\Big)\Big]^{\mathrm{T}},$$

$$S_1=\Big[-\frac{\rho u}{r},\frac{\rho(v^2-u^2)}{r},-\frac{2\rho uv}{r},-\frac{u(\rho E+p)}{r}\Big]^{\mathrm{T}},$$

ρ, p, u and v are the density, pressure, radial velocity and azimuthal velocity, respectively; $\boldsymbol{F}^{(e)}$, $\boldsymbol{G}^{(e)}$ are the convective flux terms of radial and azimuthal direction, respectively; and $\boldsymbol{S}_1$ is the source term due to the polar coordinate.

Suppose that the gases on both sides of the interface are ideal gases, the total energy per unit mass can be written as

$$E=\frac{1}{\gamma-1}\frac{p}{\rho}+\frac{1}{2}(u^2+v^2).$$

In the above formula, γ is the ratio of specific heats of ideal gas. It may be different on both sides of interface. When

the material interface changes due to the deformation by RM instability with time and space, the γ distribution will change correspondingly depending on the deformation of interface. In order to simulate the change of γ automatically, the following γ model equation [29] is adopted:

$$\Big(\frac{\partial}{\partial t}+u\frac{\partial}{\partial r}+\frac{1}{r}v\frac{\partial}{\partial\theta}\Big)\frac{1}{\gamma-1}=0. \tag{2}$$

In the numerical simulation of this paper, a unified γ was adopted since the efforts here are focused on the effect of Atwood number. The effect of γ can be found in Ref.[30].

In order to capture the moving interface, level set method [35] is used, in which the level set equation is

$$\frac{\partial\rho\varphi}{\partial t}+\frac{\partial\rho u\varphi}{\partial r}+\frac{1}{r}\frac{\partial\rho v\varphi}{\partial\theta}+\frac{\rho u\varphi}{r}=0, \tag{3}$$

where φ is the level set function. At the initial time φ is given as the signed distance distribution along the normal direction of the interface. In fact, Eq.(3) is a passive equation. At each time step the system of Eqs.(1) and (2) are solved first, then with the obtained flow field of ρ, u, v, Eq.(3) is solved to get the function φ in which the interface position is determined by the points where $\varphi=0$.

In order to make the function φ satisfy the definition of signed distance function at each time step, it is necessary to reinitialize the distribution of φ by solving the reinitializaiton equation [35, 36].

2.2 Discretization method and boundary condition

To simulate multi-scale complex flow fields accurately, high order accurate schemes are necessary. However, nonphysical oscillations may appear near discontinuities when high order schemes are used in simulation. According to the group velocity of numerical solution, the schemes can be divided into three classes, the FST(faster), MXD(mixed) and SLW(slower) schemes [35–37]. The numerical oscillations are generated before or behind the discontinuity for the FST scheme or SLW scheme, respectively. As for the MXD scheme, the components with low and moderate wave numbers in numerical solutions travel faster than the corresponding physical wave components, whereas the components with high wave numbers in numerical solutions travel slower than those of physical ones. The basic principle of the group velocity control method is that the adopted scheme must be reconstructed to make the schemes being FST/MXD behind the discontinuity, whereas being SLW before the discontinuity.

In order to improve the resolution of discontinuity, a third order accurate group velocity control scheme (GVC) was constructed in Ref.[37] to approximate the convective terms in the system of Eqs.(1-3). The GVC scheme is written as following:

$$\begin{aligned}&-\sigma^+_{j+\frac12}F_{j+1}+\Big(\frac23+\sigma^+_{j-\frac12}-\sigma^+_{j+\frac12}\Big)F_j+\Big(\frac13+\sigma^+_{j-\frac12}\Big)F_{j-1}\\&\quad=\Big(\frac56\delta^-_x+\frac16\delta^+_x\Big)f_j\quad-2\big(\sigma^+_{j+\frac12}\delta^+_x-\sigma^+_{j-\frac12}\delta^-_x\big)f_j\end{aligned}$$

$$\sigma^+_{j+\frac12}=\sigma_0\Big[1+\gamma_0 SS\big(p_{j+\frac12}\big)\Big]PP_{j+\frac12}|c|,$$

$$PP_{j+\frac12}=\Big|\frac{p_{j+1}-p_j}{p_{j+1}+p_j}\Big|$$

$$\text{and}\quad SS(p)=\operatorname{sign}\Big(\frac{\partial p}{\partial x}\frac{\partial^2 p}{\partial x^2}\Big),$$

where $F_j/\Delta x$ represents the derivative approximation of $\partial f/\partial x$, and $\sigma^+_{j+\frac12}$ is the control parameter for group velocity. The above scheme is constructed for the case of positive flux, and similar scheme can be written for the case of negative flux.

The third-order Runge-Kutta method was used to discretize the time derivatives.

To improve the resolution of the numerical solution near the moving interface, an adaptive grid refinement technique was developed in radial direction. It is implemented by the following coordinate transform for the system of Eqs.(1)–(3):

$$r=\frac{\xi_0}{A}\{\sinh[(\xi-r_0(t))\beta]+A\}, \tag{4}$$

where $r_0(t)$ is the refining position of radial mesh which represents the average position of moving interface.

Moreover, the cylindrical polar singularity was treated well by a boundary extension method. At the outer boundary far away from the center, non-reflective condition was adopted so that the outwards moving waves will not influence the inner flow fields. In the azimuthal direction, an extended periodical boundary condition was developed to ensure that uniform difference schemes were adopted when descretizing the azimuthal derivatives at grid points. Both the polar coordinate system and appropriate boundary conditions make the simulation results exhibiting good symmetry with respect to rotations about the origin. Thus all the above are essentially the ingredients of an efficient numerical method for analyzing the RM instability in the present paper.

Unlike the front tracking method [19, 26], in this paper the shock waves and interfaces are captured by the group velocity control scheme and the level set equation, respectively. Therefore, it is not necessary to introduce boundary condition across the shock waves or the fluid interface.

As for the physical parameters adopted here, we specify the units to be used in presenting our results for the numerical simulations. The dimensionless length scale and velocity are $r=\tilde r/R_0$ and $v=\tilde v/V_i$, respectively, where R_0 is the mean radius of the material interface (the radius of the unperturbed interface) at $t=0$, and V_i is the speed of the incident shock.

The initial location of the material interface is given by $r=1+a_0\sin(k\theta)$, where a_0 is the dimensionless perturbation amplitude and k is the wave number of perturbation. As for the initial physical configuration, the incident Mach number is 1.22, $a_0=0.033$ and $k=12$ for all the present simulation cases. The configuration is also shown in Fig. 1, where the imploding shock, interface and two fluids are sketched.

To validate the adopted numerical method, a grid convergence study with mesh refinement was conducted by simulating RM instability with initial density ratio equal to 5. A sequence of computations was performed starting with a

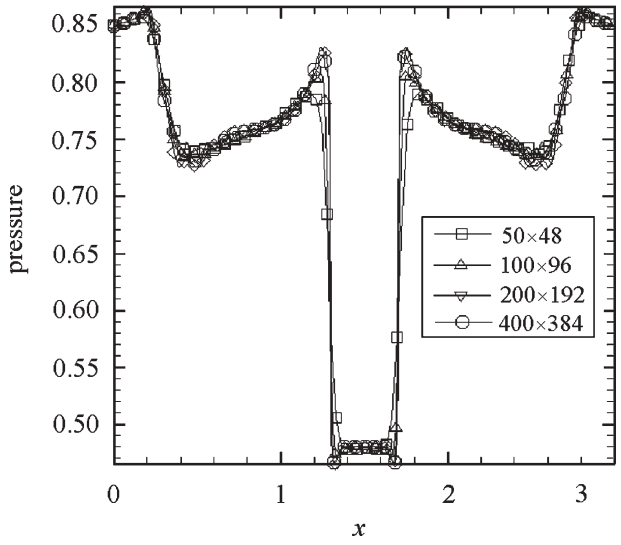

Fig. 1 Pressure distribution with different grids along a radial direction of 45° and its mirror reflection part, where the circular center is located at $x = 1.5$

resolution of 50×48 grids. Subsequent tests were made on grid systems of 100×96, 200×192 and finally 400×384. As shown in Fig. 1, the numerical solution had converged with grid system of 200×192, since there was little difference between the pressure and density at 200×192 and at 400×384. Therefore, all of the following simulations were performed with the grid system of 200×192. With the same initial configuration, Zhang obtained the grid convergence at 400×400 by a second order finite difference method on a Cartesian grid [26]. There were mainly two factors that contribute to the better convergence of the present paper. Firstly, a high-order and high-resolution group-velocity-controlling scheme was used in the numerical solution, exhibiting good resolution performance for the shock waves and the contact discontinuities. Secondly, the adaptive refinement of grid was adopted in the simulation.

3 RM instability at different Atwood numbers

The RM instability in a curved geometry has more practical application significance, especially in the field of ICF problem. In this paper, the incident shock is an imploding shock and collides with the material interface. First, the RM instability with Atwood $= -0.67$ was studied in detail in this part. Then we gave the simulation results of other three different Atwood numbers.

3.1 Evolution of the interface

The initial distribution is shown in Fig. 2(a). The fluids on both sides of interface are ideal diatomic gases with the ratio of specific heats equal to 1.4.

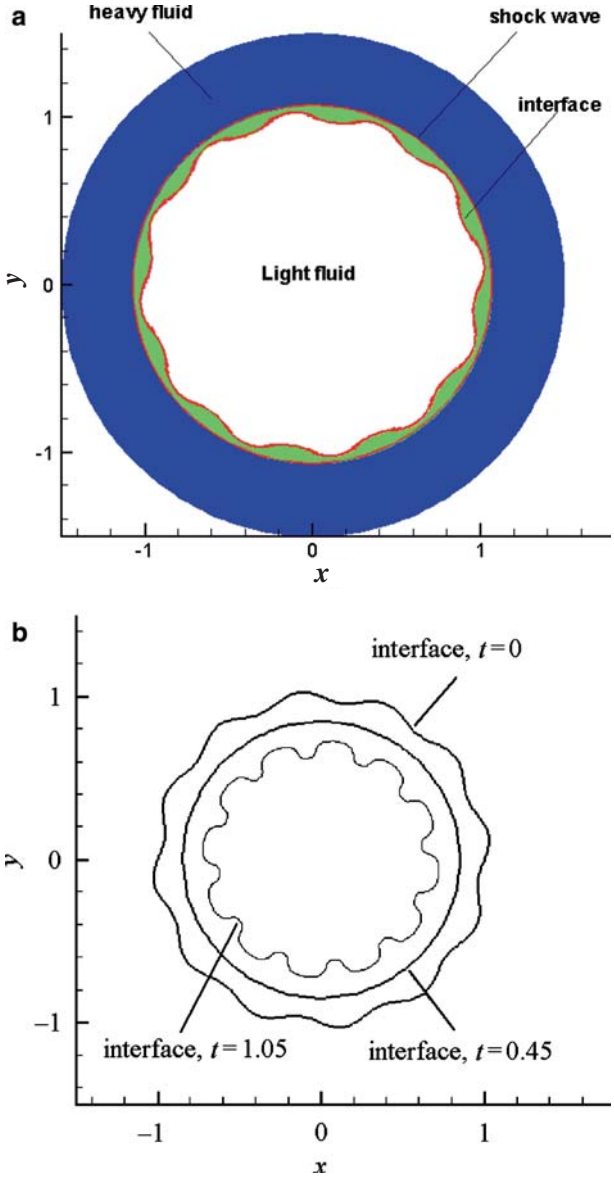

Fig. 2 (a) Initial value distribution (b) Interfaces at different time to illustrate the process of phase inversion

The Atwood number, defined as $A = (\rho_2 - \rho_1)/(\rho_2 + \rho_1)$, is a very important parameter for the RM instability analysis, where ρ_1 and ρ_2 are respectively the densities of external and internal fluid cross the incident shock wave at $t = 0$.

Now we take the case of $A = -0.67$ as an example to illustrate the evolution process of RM instability driven by an imploding shock. The corresponding density ratio of the outer fluid to the inner one is 5.

The evolution of the interface is shown in Figs. 2 and 3. When the imploding shock collides with the interface, it bifurcates into a transmitted shock moving into the inner fluid and a rarefaction wave traveling outwards. Figure 2(b) shows the interface evolution during the early stage of RM instability. Because the incident shock collides with the interface from the heavy fluid to the light one, the phenomenon

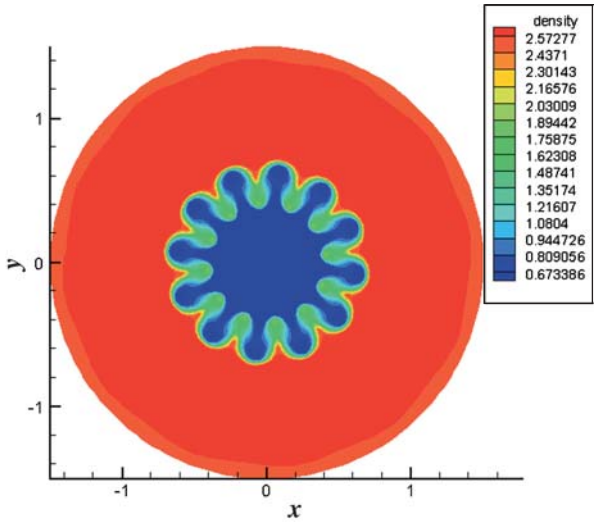

Fig. 3 Density contour at $t = 3.0(A = -0.67)$

of phase inversion occurs immediately after the collision, i.e., the initial crests and troughs of perturbed interface will exchange positions. This inversion can be observed clearly from Fig. 2(b). It is also shown that asymmetric spike and bubble structures have emerged clearly and the interface starts nonlinear evolution after phase inversion of the interface at about $t = 0.45$.

With the development of RM instability, both transmitted shock and reflected rarefaction wave are no more perfectly circular. Both of them have some angles compared with the initial circular shock, and self-intersection of waves appears. The self-intersection and interactions give rise to the so-called secondary waves which move towards the interface. The waves will influence the evolution of interface. It can be seen from the perturbation growth rate history shown in Fig. 8, where the small oscillations of growth rate are caused by the secondary waves.

When the transmitted shock traveled to the origin, it bounced from the origin with high pressure left behind. The bounced shock interacted with the interface for the second time, which was called as reshock. When the bounced shock moved from the inner light fluid into the outer heavy one, it bifurcated into a transmitted shock traveling outwards, and a reflected shock wave moving into the inner fluid. There is no phase inversion in this reshock process. The reshock accelerated the growth of perturbation at the interface, and we see the influence of reshock clearly from the growth rate history shown in Fig. 9. The reshock phenomena occurred many times with weaker and weaker intensity, and it is a special phenomenon for the RM instability in closed geometry.

Figure 3 showed the density contours at time $t = 3.0$. Fully developed nonlinear structures of the bubble and spike had been obtained. Moreover, there emerged the roll-up of spikes due to the Kelvin-Helmhlotz(KH) instability. The structures of interface became more complicated.

Moreover, Figs. 2 and 3 showed quite good symmetry with respect to rotations about the origin. The achievement of good polar symmetry would be a good justification for adopting polar coordinates.

From the results we can see that the RM instability in cylindrical geometry is similar to that of planar case in many aspects [7,19,25,27,28]. For both cylindrical and planar cases, there will be a phase inversion process when shock travels from the heavy fluid to the light one, and the interfacial perturbation grows continuously to form spikes and bubbles. However, the nonlinear effect in curved geometry manifests more evidently than in planar geometry. The results in this paper are consistent with Zhang's [26], and less grid points are adopted in our simulation due to our high resolution method. Moreover, we gave a more detailed analysis for the effect of secondary shock and reshock, also we gave the time history of the averaged interface position in Fig. 8 from which we can observe the compression history of the interface.

3.2 The effect of Atwood number

In this part we present some simulation results with different initial Atwood numbers, equal to -0.33, -0.82, and -0.90 in this section. Corresponding density ratios are 2, 10 and 20, respectively.

Some results at $t = 3.0$ for the three different Atwood numbers, -0.33, -0.82 and -0.90, were shown in Figs. 4, 5 and 6. Compared with Fig. 3, we can observe that the structure of spike and bubble, especially the spike, is closely related to the Atwood number (or density ratio). That is, the larger the absolute value of Atwood number, the longer and narrower the spike. In the case of larger absolute value of Atwood number, the inner fluid has lighter density and can be compressed more easily, thus the outer heavy fluid can penetrate into the light one deeper and sharper. Moreover, due to the lighter density of the inner fluid, the waves move faster into it so that more reshocks occurred. Thus the spikes become longer, sharper and easier to break up. This is not favorable in the

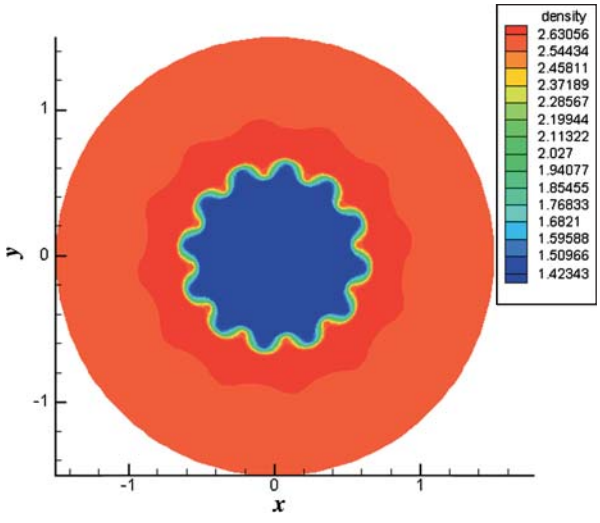

Fig. 4 Density contour at $t = 3.0(A = -0.33)$

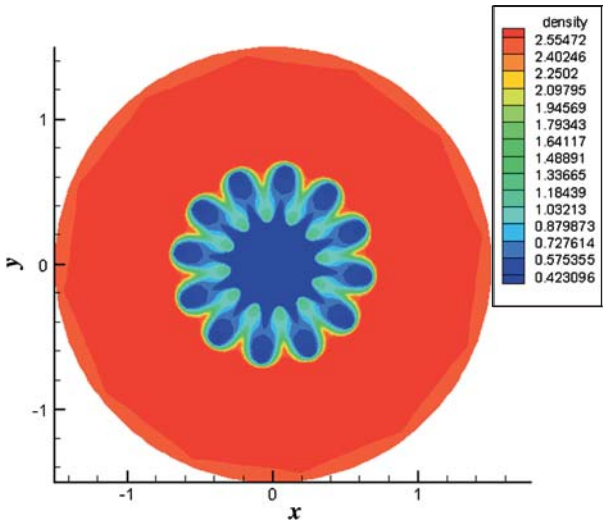

Fig. 5 Density contour at $t = 3.0(A = -0.82)$

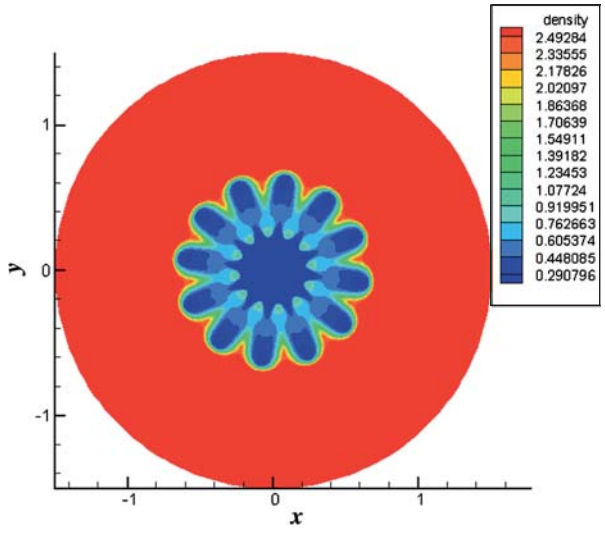

Fig. 6 Density contour at $t = 3.0(A = -0.90)$

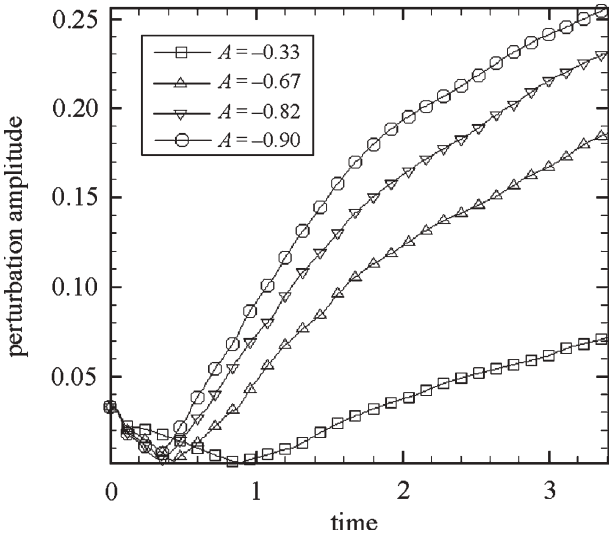

Fig. 7 Variation of perturbation amplitude vs. time at different Atwood numbers

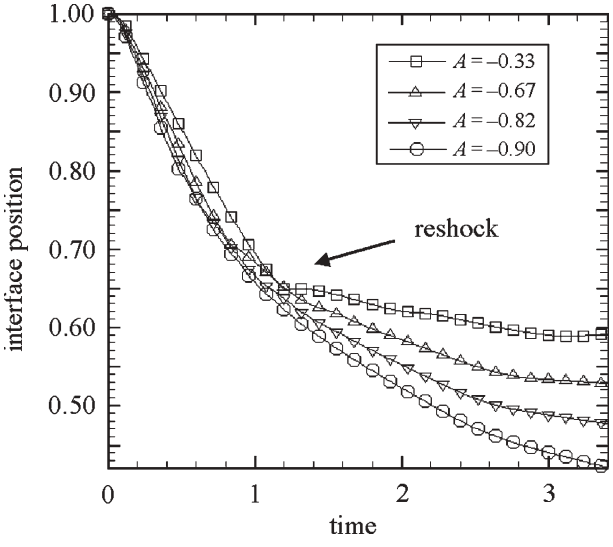

Fig. 8 Variation of averaged interface position vs. time at different Atwood numbers

application of ICF. However, for the case of $A = -0.33$, the density ratio is small, and the structures of spike and bubble are not obvious compared with other three cases.

The effect of Atwood number can also be observed from the quantitative results of interface evolution. Figure 7 shows the variation of perturbation amplitude with time, defined by $a = \frac{1}{2}(r_{\max} - r_{\min})$, where $r_{\max}$ and $r_{\min}$ are the maximum and minimum radius of interface, respectively. Figure 8 shows the variation of the average interface position with time. The growth rate of the perturbation, i.e. the time derivative of the perturbation amplitude, is shown in Fig. 9.

From Fig. 7 we can see the process of phase inversion. The amplitude decreases first and then begins to increase. With different Atwood numbers, the phase inversion period is different. The larger the absolute value of Atwood number, the shorter the phase inversion period. The development of perturbation amplitude also reveals similar relationship between the Atwood numbers and the above-mentioned spikes. The larger absolute value of Atwood number, the larger the amplitude. In the case of $A = -0.90$, the phase seems to invert earlier than in the case of $A = -0.67$, and even much earlier than in the case of $A = -0.33$. With earlier phase inversion, the amplitude will be larger. In the case of $A = -0.33$ with the longest inversion period, the amplitude will take longer time to grow because it is later to start growing.

Figure 8 shows the history of the average material interface location. It implies how much the inner fluid is compressed. The larger the Atwood number, the more the inner fluid compessed. At early time, the four cases have about the same compression ratio since they have the same incident

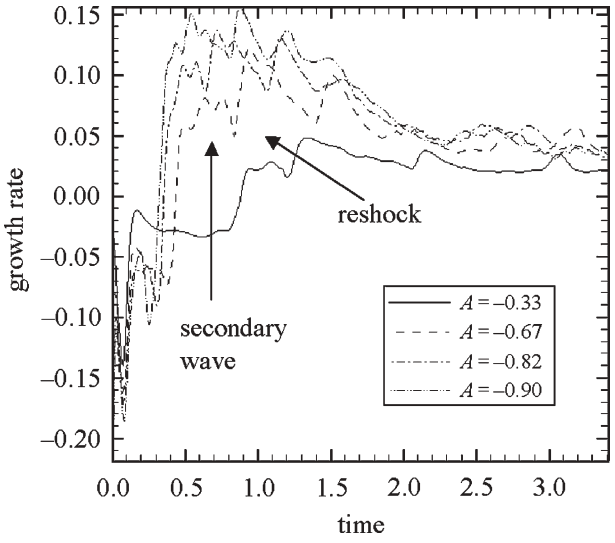

Fig. 9 Variation of perturbation growth rate vs. time at different Atwood numbers

shock wave with Mach number equal to 1.22. At later time, the reshocked waves reflected from the origin restrain the compression process.

Figure 9 shows that the growth rate of perturbation grows quickly in the early stage and reaches the maximum at about $t = 1.0$ except for the case of $A = -0.33$. After $t = 1.0$ or so, the growth rate decays gradually. In the early stage, the larger the absolute value of Atwood number, the larger the growth rate. However, after $t = 1.0$, the four cases except for the one of $A = -0.33$ show almost the same growth rate and seem to be independent of Atwood number. According to the impulsive model or linear theory for planar case, the growth rate is proportional to the Atwood number. However, in the imploding case, it shows different relationship with Atwood number. The nonlinear effect of the RM instability is more evident except for the case of $A = -0.33$, and the growth rate decays because of nonlinear effects as predicted by nonlinear theories [7, 15, 17]. The case of $A = -0.33$ has no evident decaying trend, and shows different feature as compared with other three. In conclusion, we can infer that there should be a sophisticated relationship between the Atwood number and the inversion period or the growth rate.

Zhang, Dutta, et al. [16, 26, 33] investigated the effect of inflow Mach number by numerical simulation. In their paper, only one kind of density ratio was considered. As far as we know, the effect of Atwood number on the RM instability has not been studied in curved geometry. According to the linear theory for planar cases, the growth rate is proportional to the Atwood number. Here, from simulation we find the linear theory not tenable in curved geometry even in the early stage. This means that new models need to be proposed for the RM instability in curved geometry. Furthermore, we find that Atwood number has an important effect on the phase inversion process.

4 Conclusions

In this paper, an efficient numerical method was developed to simulate the RM instability in curved geometry. The analysis of simulation results shows that the Atwood number (or density ratio) plays an important role in the development of RM instability. The larger the absolute value of Atwood number, the larger the perturbation amplitude. With different Atwood numbers, the bubble and spike structure exhibits different shapes. Furthermore, the effect of Atwood number can be observed from the quantitative results of the interface evolution, such as the variation of perturbation amplitude, growth rate and averaged interface position versus time. The simulation results in later stage have some limitations due to the adopted two-dimensional numerical method. We expect to perform three-dimensional numerical investigation of the RM instability in the near future.

References

1. Richtmyer, R.D.: Taylor instability in shock acceleration of compressible fluids. Commun. Pure Appl. Maths. **13**, 297–319 (1960)
2. Meshkov, E.E.: Instability of a shock wave accelerated interface between two gases. NASA Tech. Trans. **F-13**, 074 (1970)
3. Cohen, R.H., Dannevik, W.P., Dimits, A.M., Eliason, D.E., Mirin, A.A., Zhou, Y.: Three-dimensional simulation of a Richtmyer-Meshkov instability with a two-scale initial perturbation. Phys. Fluids. **14**, 3692–3709 (2002)
4. Yang Y., Zhang Q., Sharp D.H.: Small amplitude theory of Richtmyer-Meshkov instability. Phys. Fluids. **6**, 1856–1873 (1994)
5. Velikovich, A.L.: Analytic theory of Richtmyer-Meshkov instability for the case of reflected rarefaction wave. Phys. Fluids. **8**(6), 1666–1679 (1996)
6. Velikovich, A.L., et al: Richtmyer-Meshkov-like instabilities and early-time perturbation growth in laser targets and Z-pinch loads. Phys. Plasmas. **7**(5), 1662–1671 (2000)
7. Brouillette, M.: The Richtmyer-Meshkov instability. Annu. Rev. Fluid Mech. **34**, 445–468 (2002)
8. Sturtevant, B.: Rayleigh-Taylor instability in compressible fluids. In: Gronig H. (ed) Proceedings International Symposium Shock Tubes Waves, 16th, aachen, VCH Verlag, Basel, 1987
9. Mikaelian, K.O.: Growth rate of the Richtmyer-Meshkov instability at shocked interfaces. Phys. Rev. Lett. **71**, 2903–2906 (1993)
10. Vandenboomgaerde, M., Mugler, C., Gauthier, S.: Impulsive model for the Richtmyer-Meshkov instability. Physical Review E. **58**, 1874–1882 (1998)
11. Wouchuk, J.G., Nishihara, K.: Asymptotic growth at a shocked interface. Phys. Plasmas **3**, 3761–3776 (1997)
12. Wouchuk, J.G., Carretero, R.: Linear perturbation growth at the trailing edge of a rarefaction wave. Phys. Plasmas **10**, 4237–4252 (2003)
13. Zabusky, N.J.: Vortex paradigm for accelerated inhomogeneous flows: visiometrics for the Rayleigh-Taylor and Richtmyer-Meshkov enviroments. Annu. Rev. Fluid Mech. **31**, 495–536 (1999)
14. Fraley, G.: Rayleigh-Taylor stability for a normal shock wave-density discontinuity interactinon. Phys. Fluids **29**, 376–386 (1986)
15. Alon, U., Hecht, J., Ofer, D., Shvarts, D.: Power laws and similarity of Rayleigh-Taylor and Richtmyer-Meshkov mixing fronts at all density ratios. Phys Rev. Lett. **74**, 534–537 (1995)
16. Zhang, Q., Graham, M.J.: Scaling laws for unstable interface driven by strong shocks in cylindrical geometry. Phys. Rev. Lett. **79**, 2674–2677 (1997)
17. Zhang, Q., Sohn, S.I.: Nonlinear theory of unstable fluid mixing driven by shock wave. Phys. Fluids **9**, 1106–1124 (1997)

18. Fu, D.X., Ma, Y.W.: A high order accurate difference scheme for complex flow fields. J. Comput. Phys. **134**, 1–15 (1997)
19. Holmes, R.L., et al.: Richtmyer-Meshkov instability growth: experiment, simulation and theory. J. Fluid Mech. **389**, 55–79 (1999)
20. Li, X.L., Zhang, Q.: A comparative numerical study of the Richtmyer-Meshkov instability with nonlinear analysis in two and three dimensions. Phys. Fluid **9**, 3069–3077 (1997)
21. Brouillette, M.: Experiments on the Richtmyer-Meshkov instability: single-scale perturbations on a continuous interface. J. Fluid Mech. **263**, 271–292 (1994)
22. Dimonte, G., Frerking, C.E., Schneider, M., Remington, B.: Richtmyer-Meshkov instability with strong radiatively driven shock. Phys. Plasmas **3**, 614–630 (1996)
23. Dimonte, G., Remington, B.: Richtmyer-Meshkov experiments on the nova laser at high compression. Phys. Rev. Lett. **70**, 1806–1809 (1993)
24. Cloutman, L.D., Wehner, M.F.: Numerical simulation of Richtmyer-Meshkov instabilities. Phys. Fluid **4**, 1821–1830 (1992)
25. Mugler, C., Gauthier, S.: Numerical simulations of single-mode Richtmyer-Meshkov experiments. Physical Review E **58**, 4548–4555 (1998)
26. Zhang, Q., Graham, M.J.: A numerical study of Richtmyer-Meshkov instability driven by cylindrical shocks. Phys. Fluids **10**, 974–992 (1998)
27. Holmes, R.L., Grove, J.W., Sharp, D.H.: Numerical investigation of Richtmyer-Meshkov instability using front tracking. J. Fluid Mech. **301**, 51–64 (1995)
28. Zabusky, N.J., Kotelnikov, A.D., Gulak, Y., Peng, G.Z.: Amplitude growth rate of Richtmyer-Meshkov unstable two-dimensional interface to intermediate times. J. Fluid Mech. **475**, 147–162 (2003)
29. Shyue, K.M.: An efficient shock-capturing algorithm for compressible multicomponent problems. J. Comput. Phys. **142**, 208–242 (1998)
30. Tian, B.L., Fu, D.X., Ma, Y.W.: Effects of adiabatic exponent on Richtmyer-Meshkov instability. Chin. Phys. Lett. **21**, 1770–1773 (2004)
31. Oron, D., et al.: Dimensionality dependence of the Rayleigh-Taylor and Richtmyer-Meshkov instability late-time scaling laws. Phys. Plasmas **8**, 2883–2889 (2001)
32. Zhou, Y., et al.: Progress in understanding turbulent mixing induced by Rayleigh-Taylor and Richtmyer-Meshkov instabilities. Phys. Plasmas **10** 1883–1896 (2003)
33. Duttaa, S., Glimm, J., Grove, J.W., Sharp, D.H., Zhang, Y.M.: Spherical Richtmyer-Meshkov instability for axisymmetric flow. Mathematics and Computers in Simulation **65**, 417–430 (2004)
34. Glimm, J., Grove, J., Zhang, Y.M., Dutta, S.: Numerical study of axisymmetric Richtmyre-Meshkov instability and azimuthal effect on spherical mixing. J. Stat. Phys. **107**, 241–260 (2002)
35. Osher, S., Fedkiw, R.P.: Level set methods: an overview and some recent results. J. Comput. Phys. **169**, 463–502 (2001)
36. Zhuang, F.G.: On numerical techniques in CFD. Acta Mechanica Sinica **16**(3), 193–216 (2000)
37. Tian, B.L., Fu, D.X., Ma, Y.W.: Group velocity control scheme and two-dimensional riemann solver. Chin. J. Comput. Mech. **22**(1), 104–108 (2005)